



**HAL**  
open science

## Mid-Infrared HgTe/As<sub>2</sub>S<sub>3</sub> Field Effect Transistors and Photodetectors

Emmanuel Lhuillier, Sean Keuleyan, Pavlo Zolotavin, Philippe Guyot-Sionnest

► **To cite this version:**

Emmanuel Lhuillier, Sean Keuleyan, Pavlo Zolotavin, Philippe Guyot-Sionnest. Mid-Infrared HgTe/As<sub>2</sub>S<sub>3</sub> Field Effect Transistors and Photodetectors. *Advanced Materials*, 2013, 25 (1), pp.137 - 141. 10.1002/adma.201203012 . hal-01438562

**HAL Id: hal-01438562**

**<https://hal.science/hal-01438562>**

Submitted on 25 Aug 2020

**HAL** is a multi-disciplinary open access archive for the deposit and dissemination of scientific research documents, whether they are published or not. The documents may come from teaching and research institutions in France or abroad, or from public or private research centers.

L'archive ouverte pluridisciplinaire **HAL**, est destinée au dépôt et à la diffusion de documents scientifiques de niveau recherche, publiés ou non, émanant des établissements d'enseignement et de recherche français ou étrangers, des laboratoires publics ou privés.

## Mid-Infrared HgTe/As<sub>2</sub>S<sub>3</sub> FETs and photodetectors.

Emmanuel Lhuillier, Sean Keuleyan, Pavlo Zolotavin and Philippe Guyot-Sionnest

*James Franck Institute, 929 E. 57<sup>th</sup> Street, The University of Chicago, Chicago, Illinois  
60637, USA*

**Abstract:** Colloidal quantum dots (CQDs) with mid-infrared (IR) tunable bandgaps present a new paradigm for mid-IR materials, but advances in charge transport and collection are needed for practical use in electronic applications. By replacing the organic ligands in films of HgTe CQDs with As<sub>2</sub>S<sub>3</sub>, a problem of oxidation in air is avoided and charge carrier mobilities are improved 100 fold compared to the standard organic ligand exchange. The composite inorganic HgTe/As<sub>2</sub>S<sub>3</sub> material allows for ambipolar field effect transistors with on-off ratios up to 10<sup>7</sup>, and photodetectors with high sensitivity, reaching 3x10<sup>10</sup> Jones at 230 K with a 3.5 micron cutoff wavelength.

**Keywords:** HgTe, As<sub>2</sub>S<sub>3</sub>, colloidal quantum dot, inorganic matrix, FET, mid-IR, photodetection

Optoelectronic devices based on colloidal quantum dots (CQDs) benefit from low-cost solution preparation and processing, and have been extensively investigated.<sup>[1]</sup> Much work to-date has focused on visible emitters, primarily for use in visible displays and bio-labeling,<sup>[2]</sup> and near-IR absorbers<sup>[3]</sup> for solar cells,<sup>[4]</sup> and photodetectors.<sup>[567]</sup> Inorganic CQDs have an unrealized advantage further into the mid-and far-infrared, where no other solution-processable materials are available. Furthermore, since high-cost epitaxially-grown materials

dominate mid-infrared applications, the development of CQDs as a low-cost technology could open new markets.

Quantum dots of HgTe, a semi-metal in the bulk, could in principle have bandgaps tunable through the full infrared range by controlling the size. The synthesis<sup>[8]</sup> and optical properties<sup>[9]</sup> of HgTe CQDs with bandgaps tunable through the mid-infrared range of 3-5  $\mu\text{m}$  (0.2 to 0.5eV) were recently reported. Particles with diameters between 6 and 12 nm have been prepared and the monodisperse samples show sharp absorption and photocurrent spectral edges, as shown in *Figure 1(a)*. Competitive photodetection sensitivities, however, will require the elimination of the mid-IR absorption from the organic ligands, as along with improvements in charge transport and collection as well as reduced noise.<sup>[10]</sup>

Initial strategies for improving mobilities relied on organic ligand exchange of preformed films of CQDs<sup>[11,12,13]</sup> To produce fully-inorganic composite materials, a number of reports have been published on the use of solution phase inorganic ligands, providing a variety of choices for passivation and barrier control.<sup>[14,15,16,17,18]</sup> Arsenic sulfide, in addition to its use as an inorganic ligand<sup>[19,20]</sup> has been used as an infrared-transparent inorganic matrix, with advantages for the near-infrared photoluminescence of PbS/CdS core/shell quantum dots.<sup>[21]</sup> In this paper, we use a ligand exchange procedure with arsenic sulfide on films of monodisperse HgTe CQDs and compare the results with organic ligand exchange.

Simply dried films of the monodisperse HgTe CQDs are highly insulating, due to the long alkane ligands, which include octadecylamine, trioctylphosphine, and dodecanethiol. After ligand exchange by dipping the films in a solution of ethanedithiol in ethanol, the films become photoconductive. The photoresponse and optical properties of films of these organic-inorganic composite materials, have been reported.<sup>[9]</sup>

Exchange performed in air with other ligands is also explored, including thiols (1,2-ethanedithiol, 1,4-benzenedithiol, 1,4-butanedithiol) and amines (propylamine, butylamine, butanediamine, 1,7-heptanediamine). While ethanedithiol provides the best response, all ligands tested lead to photoconductive films. However the dark current  $I(T)$  curves show that all films exhibit a non-monotonic current as a function of temperature with a more or less prominent bump around 200K, as seen in Figure 1 (b) and (c). Such behavior had not been observed for the films made with aggregated HgTe CQDs<sup>[22]</sup> and since both thiol and amine ligands lead to a similar feature in the  $I(T)$  curve, the feature is not specific to the ligands. The responsivity of the films to infrared illumination is low, ranging from  $10\mu\text{A}\cdot\text{W}^{-1}$  to  $5\text{mA}\cdot\text{W}^{-1}$  (Figure 1(d)). Although a photocurrent spectral response was measurable with a standard scanning FTIR (Figure 1 (a)), the responsivity is two decades lower than with the previous aggregated HgTe CQDs.

While performing experiments with a sample in the vacuum of the cryostat, the bump was observed to decrease in magnitude over a period of days but then rapidly recovered upon exposure to air. Suspecting oxidation,<sup>[23]</sup> samples were prepared in a nitrogen-filled glove box and transferred in a closed cell to the cryostat. With such air-free preparation and transfer, the  $I(T)$  curve is monotonic, with an Arrhenius activation energy close to half of the optical band gap in the higher temperature range, see (Figure 1(b)).

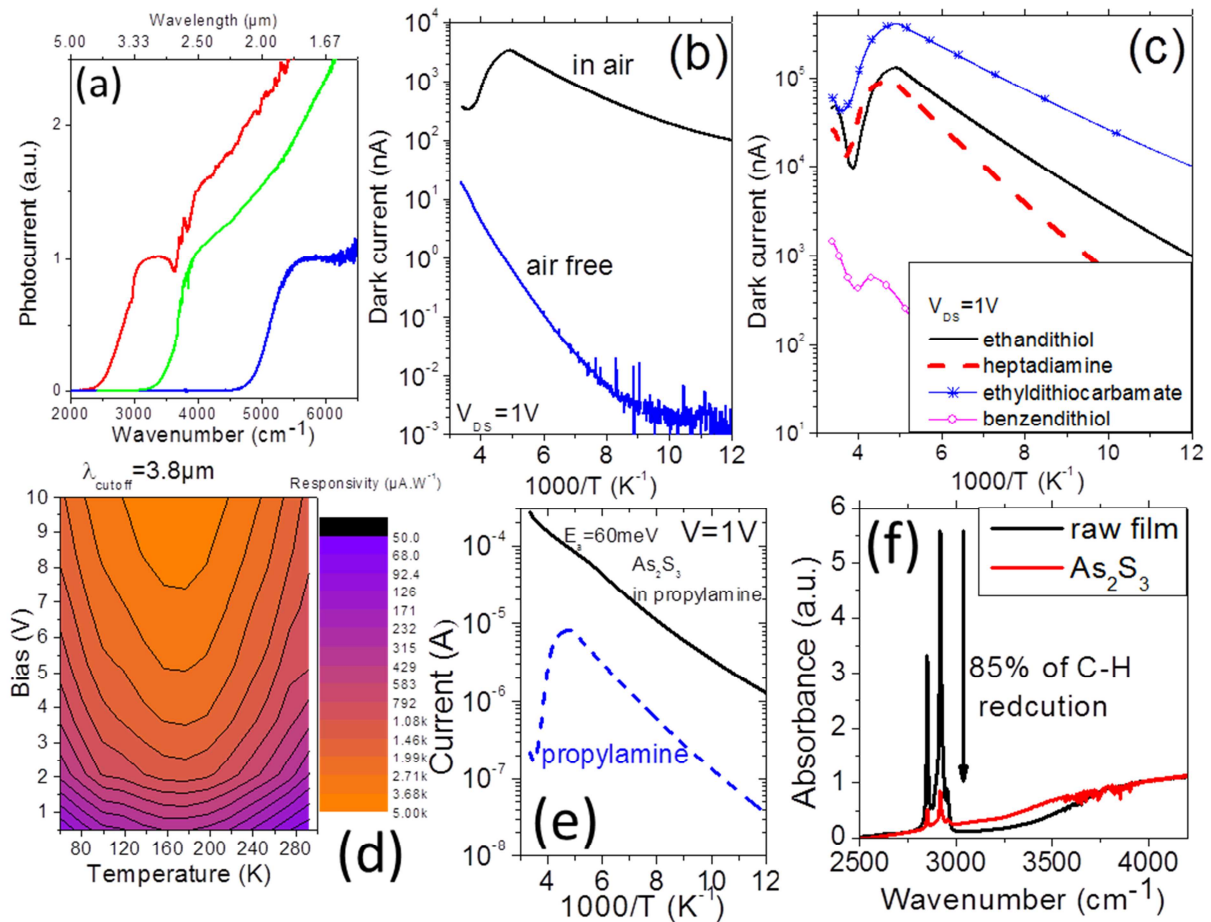


Figure 1 (a) Typical photocurrent spectra of HgTe CQDs after ligand exchange, the reddest spectrum is associated to 12nm large particle while the bluest spectrum is due to 6nm large CQD (b) Current as a function of temperature for a film of HgTe CQD processed with ethanedithiol in air and air-free. (c) Current as a function of temperature for HgTe CQD film processed in air with different ligands (d) Responsivity map of a HgTe CQD film processed with ethanedithiol in air as a function of bias and temperature. (e) Current as a function of the inverse of the temperature for a HgTe CQD film processed with  $As_2S_3$  in air (f) Absorption spectra of a film of HgTe CQD unprocessed and after ligand exchange with the  $As_2S_3$  solution.

It was then concluded that the films made from the monodisperse HgTe CQDs need to be processed and kept in air-free conditions. Presumably, the surfaces are more exposed than with the aggregated HgTe CQDs reported earlier, leading to increased sensitivity to oxidation

which then leads to the formation of acceptor levels. It is also noted that although the air-free process with EDT decreased the dark current, it did not improve the responsivity significantly. We then explored the inorganic ligand exchange route.  $\text{As}_2\text{S}_3$  is an infrared glass that can be easily dissolved in the low boiling point propylamine and is used to make infrared transparent sol/gel films.<sup>[24]</sup> Recently Kovalenko *et al* showed that the organic ligands on PbS/CdS nanoparticles could be replaced by such an  $\text{As}_2\text{S}_3$  solution for transparent  $\text{As}_2\text{S}_3$  films with dispersed fluorescent PbS/CdS particles.<sup>21</sup> While this is advantageous for making luminescent films, the dilute dispersion of the particles in the matrix reduces the optical absorption of the films, and the wide bandgap of  $\text{As}_2\text{S}_3$  renders the films insulating.

To make photoconductive films, the strategy pursued here mimics organic ligand exchange procedures. The drop-cast HgTe QD films are dipped in a dilute solution of  $\text{As}_2\text{S}_3$  and propylamine in ethanol and then dried at room temperature. The concentration of  $\text{As}_2\text{S}_3$  and propylamine in ethanol needs to be optimized, as at high concentrations, the resulting films are very conductive but without photoresponse, while saturated  $\text{As}_2\text{S}_3$  in propylamine (without ethanol) delaminates the film.

The C-H stretch absorption band is strongly reduced by this process, showing that most of the organic ligands are replaced (see Figure 1(f)).

When performed in air, this process leads to a large dark current with an activation energy of 50 to 60meV which is much smaller than half the optical band gap, see Figure 1 (e). The photoresponse is also very slow (> seconds, see supplementary information), which can be assigned to long lived traps. When the films of HgTe CQD are processed with  $\text{As}_2\text{S}_3$  in air-free conditions, the I(T) curve indicates that the intrinsic behavior is recovered, just like for the air-free ligand exchange with EDT. As shown in Figure 2 (a), the I(T) curve is monotonic and the activation energy is close to half the optical band gap.

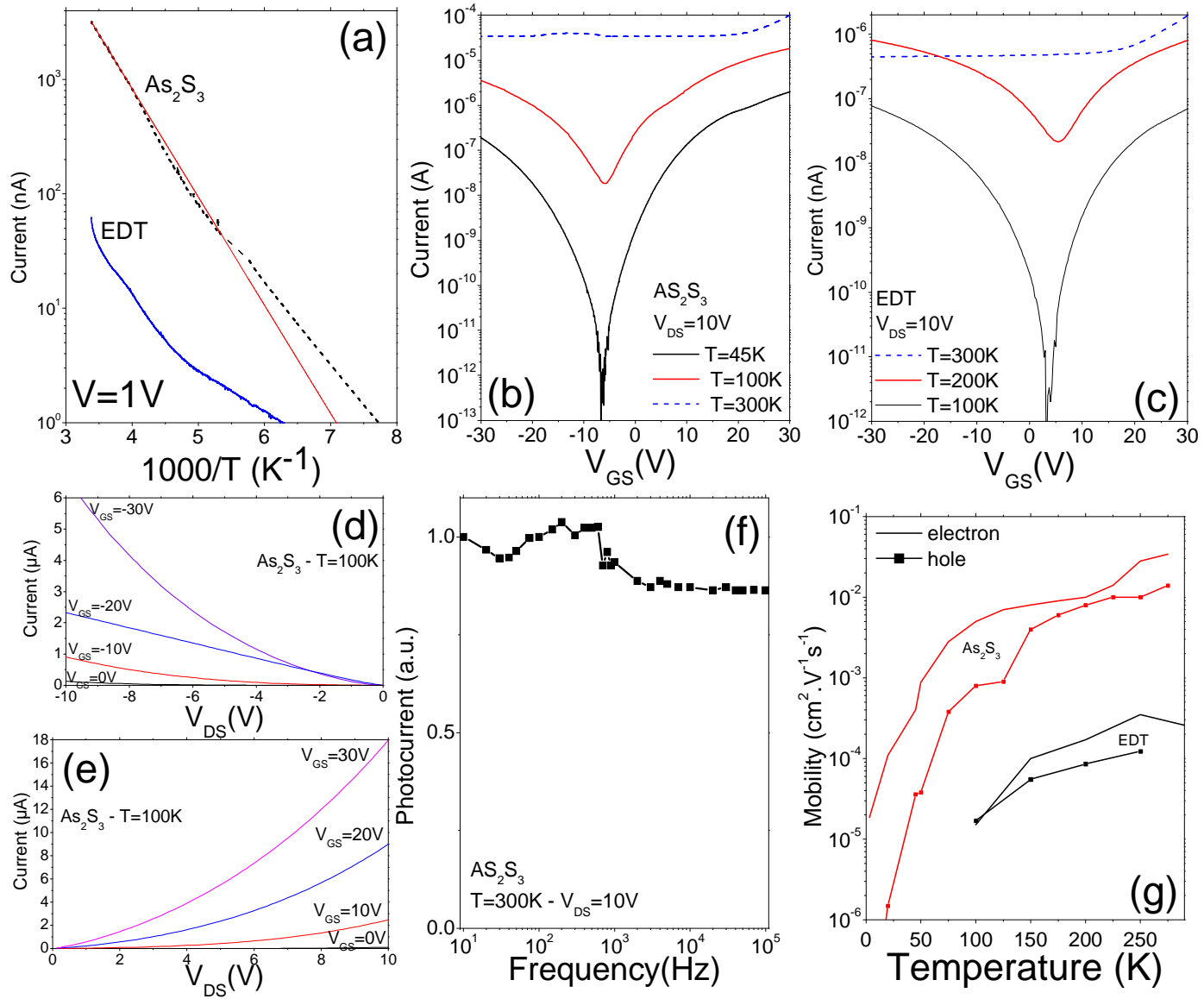


Figure 2 (a) Current as a function of the temperature for a film processed air-free after ligand exchange with ethanedithiol (blue line) and  $\text{As}_2\text{S}_3$  (dashed line), under 1V bias. The red line is an Arrhenius fit, where the activation energy is half the optical gap. (b) Current as a function of gate bias for a HgTe CQD film processed with  $\text{As}_2\text{S}_3$  under 10V source drain bias at different temperatures. (c) Current as a function of the gate bias for a HgTe CQD film processed with EDT, under 10V source drain bias at different temperatures. (d) Current as a function of source-drain bias for a HgTe CQD film processed with  $\text{As}_2\text{S}_3$ , at 100K and under different negative gate biases. (e) Current as a function of source-drain bias for a HgTe CQD

*film processed with As<sub>2</sub>S<sub>3</sub> at 100K under different positive gate biases (f) Photocurrent signal of a HgTe CQD film processed with As<sub>2</sub>S<sub>3</sub> as a function of the frequency of incident modulated light. (g) Electron and hole mobilities of a HgTe CQD film processed with As<sub>2</sub>S<sub>3</sub> and EDT as a function of temperature.*

To confirm the intrinsic character of the films of HgTe CQDs and to determine carrier mobilities, field effect transistor (FET) devices were made. Kim and coworkers previously reported FETs with HgTe CQDs [25,26]. Thin films of HgTe CQD annealed at 150°C, were reported to be p-type, with on-off ratios up to 10<sup>3</sup> and mobility up to 1cm<sup>2</sup> V<sup>-1</sup>s<sup>-1</sup>. However no study of their infrared optical absorption edge or photoresponse were reported.<sup>27</sup>. Our FETs are made from the HgTe CQD films and processed at room temperature to preserve the optical absorption edge. When films are processed air-free, they are ambipolar, consistent with their intrinsic behavior seen in the I(T) curves. At low temperatures, the FET show high on-off ratios up to 10<sup>7</sup> for As<sub>2</sub>S<sub>3</sub>-processed films, and 10<sup>6</sup> for EDT processed films, see Figure 2 (b) (c) (d) and (e). At room temperature, the on-off ratio is much smaller, and this is attributed to thermally activated carriers.

Carrier mobilities in Figure 2 (g) are obtained from the I<sub>DS</sub>(V<sub>GS</sub>) curves using the relation

$$\mu_n^{FET} = \frac{L}{WC_\Sigma V_{DS}} \left. \frac{\partial I_{DS}}{\partial V_{GS}} \right)_{V_{DS}}$$

Where  $L$  is the electrode spacing (10μm),  $W$  is the electrode length (25×2.5mm),  $C_\Sigma$  the surface capacitance equal to 34.5μF.m<sup>-2</sup> for the 1μm thick SiO<sub>2</sub> and  $V_{DS}$  the drain source bias.

Hole and electron mobilities with EDT are similar to previous results where carriers were injected electrochemically<sup>[28]</sup>. For the film processed with As<sub>2</sub>S<sub>3</sub>, μ~ 10<sup>-2</sup>cm<sup>2</sup>V<sup>-1</sup>s<sup>-1</sup> while with EDT μ~10<sup>-4</sup>cm<sup>2</sup>V<sup>-1</sup>s<sup>-1</sup>. This 100 fold improvement in mobility readily explains the improved properties of the As<sub>2</sub>S<sub>3</sub> treated films. It is instructive to consider the associated hopping time

given by  $\tau_{hop} \approx \frac{ea^2}{6\mu k_B T}$  (with  $a$  the interparticle center to center distance) which at room temperature is 0.65 ns with  $As_2S_3$  and 65 ns with EDT. The competition between the hopping time and the nonradiative lifetime is key to efficient charge separation. Although the non-radiative lifetime is unknown at present, the 100-fold increased responsivity with  $As_2S_3$  shown in Figure 3 (a) and (c), which tracks the improvement in the mobility, suggests that a faster hopping time would still be beneficial.

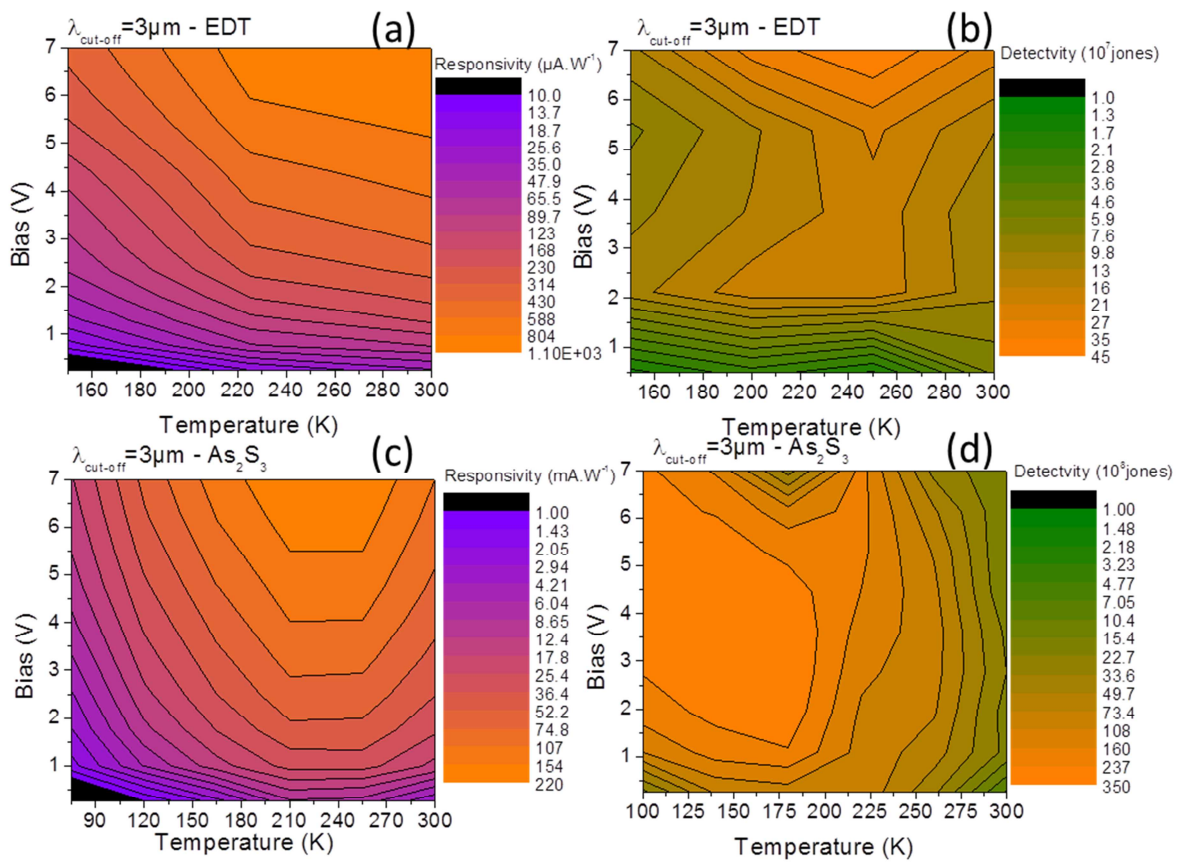


Figure 3 (a) Responsivity map as a function of bias and temperature for a film of HgTe CQD treated with ethanedithiol. (b) Detectivity map as a function of bias and temperature for a film of HgTe CQD treated air free with ethanedithiol. (c) and (d) are respectively the responsivity map and detectivity map of the same HgTe CQDs but processed with  $As_2S_3$  at 1kHz.

From the dark noise measurements, the  $\text{As}_2\text{S}_3$  films also show also much improvement in the detectivity with a value higher than  $10^{10}$  jones at 1kHz for a film with a 3.5  $\mu\text{m}$  cut-off at 230 K, shown in Figure 3 (b) and (d). This value of the detectivity is 30 times higher than with the aggregated material<sup>[10]</sup>. With further optimization, the  $\text{As}_2\text{S}_3$  ligand exchange approach is likely to lead to improvements for detector materials at longer wavelengths as well. Moreover, the photoconductivity of the film processed with  $\text{As}_2\text{S}_3$  remains fast, with a flat frequency response between 10Hz and 100kHz, as shown in Figure 2 (f).

With the HgTe CQD films, processed air-free with  $\text{As}_2\text{S}_3$ , the ambipolar behavior remains even when the film is exposed to air (see supplementary information). Thus, HgTe/ $\text{As}_2\text{S}_3$  is more stable to oxidation compared to all tested organic ligands. It is expected that the glassy  $\text{As}_2\text{S}_3$  matrix slows down the diffusion of  $\text{O}_2$  or  $\text{H}_2\text{O}$  compared to the organic ligands. This is an additional significant benefit of the inorganic  $\text{As}_2\text{S}_3$  ligand exchange. In addition, a thicker encapsulating layer of  $\text{As}_2\text{S}_3$  can be deposited on top of the CQD films to provide further protection of the films.<sup>29</sup> At present the films have been prepared at room temperature by slow drying of the  $\text{As}_2\text{S}_3$  sol-gel. It is likely that further improvement in the detector properties will be achieved with a careful annealing procedure.

In summary, monodisperse HgTe CQDs have a well defined optical response in the mid-IR but conductive films required an appropriate ligand exchange. Different organic ligands were investigated, where it was found that ligand exchange in air leads to p-type conduction and larger dark current, attributed to acceptor levels arising from oxidation. Intrinsic behavior is obtained when the samples are processed under nitrogen. The best organic ligand, ethanedithiol, leads to only moderate performances with detectivity of  $10^8$  jones, and this can partly be assigned to the low mobility of  $10^{-4}$   $\text{cm}^2/\text{Vs}$ . Using air-free ligand exchange in

solutions of  $\text{As}_2\text{S}_3$  leads to intrinsic material and the extensive removal of organics. FET measurements show ambipolar mobility of  $\sim 10^{-2}\text{cm}^2/\text{Vs}$  with high on-off ratios at low temperatures. Once encapsulated in  $\text{As}_2\text{S}_3$ , the films are stable against oxidation in air. Responsivity greater than  $100 \text{ mA}\cdot\text{W}^{-1}$  and a detectivity of  $3.5 \times 10^{10}$  jones have been obtained at 3.5 microns and 230K. Inorganic ligand exchange and encapsulation is a promising method for improving both the electrical and optical properties of the quantum dot films. These results with  $\text{HgTe}/\text{As}_2\text{S}_3$  motivate further work on infrared transparent inorganic matrices, improved detectors, and possibly emitters at longer wavelengths.

## **EXPERIMENTAL SECTION**

- **Material synthesis**

$\text{HgTe}$  CQDs were prepared following ref. 8. Octadecylamine (ODA) was used in place of oleylamine, as some batches of the technical grade (70%) oleylamine were found to result in larger particle size distributions. A 1M solution of Te in trioctylphosphine (TOP) is prepared ahead of time by agitating at room temperature for several days in a glove box. In a typical synthesis, 135 mg of  $\text{HgCl}_2$  and 7.4g of ODA are added to a three-neck flask, flushed several times with Ar, heated under vacuum to  $120^\circ\text{C}$  for 1 hour then cooled under Ar to  $80^\circ\text{C}$ . 0.5mL of the 1M Te in TOP is then quickly injected. The solution darkens over a period of about 20 s, indicating the formation of  $\text{HgTe}$ . After an appropriate growth time, a solution of 10% (vol.) dodecanethiol in TCE is quickly injected and heating is removed. The reaction mixture is stirred several minutes before precipitating with methanol. After centrifugation, the precipitate is redispersed in toluene and precipitated at least three additional times. Finally the nanoparticles are stored in TCE or in a 9:1 in volume mixture of hexane:octane, in the glovebox.

- **Film preparation and characterization**

Films are prepared by drop-casting the hexane-octane solution of CQDs onto interdigitated electrodes. Different electrodes are used for the photoconductive and the FET measurements. For photoconductive measurements, electrodes (ABTech IME 1050) with 50 periods of Pt interdigitated electrodes (5 mm long and 10  $\mu\text{m}$  spacing) are used. The spectral response is acquired using a FTIR Nicolet magna IR 550, while the device is biased and the signal amplified using a femto DLCPA 200 amplifier.

For FET measurements, gold interdigitated electrodes were deposited on a doped silicon substrate with a 1  $\mu\text{m}$  thick oxide layer. Films are mounted on the cold finger of a closed cycle helium cryostat (ColdEdge SDRK-101D) with a CryoCon 32B temperature controller. Transport measurements are made using a Keithley 6487 picoammeter. For FET measurements, a National Instruments acquisition board (BNC 2110), amplified 10 times, is used to apply the gate bias.

Responsivity is measured using a blackbody (Omega BB-4A operating at 1255K) as a broadband photon source. The light is chopped at 25Hz and a Ge plate cuts the illumination below 1.7 $\mu\text{m}$ . The device is biased and the signal is amplified using a femto DLCPA 200 amplifier. The modulation is monitored on a Tektronix, TDS 1012B oscilloscope. The frequency response of the photocurrent is measured by illuminating the sample with a 800nm laser diode modulated with a signal generator up to 100 kHz.

Dark noise measurements are made by biasing the sample and amplifying the signal with a femto DLCPA 200 amplifier. The output signal is high-pass filtered (with a 0.1Hz cut-off frequency RC filter) and amplified ten times using an operational amplifier. Finally the current spectral density is obtained with a Stanford research SR 760 spectrum analyzer.

Transmission electron microscopy (TEM) and scanning electron microscopy (SEM) are made using respectively FEI Technai F30 and FEI nova nanoSEM 200. A Bruker D8 diffractometer is used for X ray powder diffraction measurements and a Nicolet magna IR 550 FTIR for optical spectroscopy in the infrared

## SUPPORTING INFORMATION

Supporting information includes (i) information on chemicals used (ii) HgTe CQD characterization (iii) information about the noise setup (iv) effect processing with AsCl<sub>3</sub>. (v) Effects of processing with As<sub>2</sub>S<sub>3</sub> in air and (vi) Effects of oxidation on a sample prepared air-free with As<sub>2</sub>S<sub>3</sub> (vii) responsivity and detectivity map of sample with cut-off wavelength at 2 μm.

## ACKNOWLEDGEMENTS

This work is supported by the DARPA COMPASS program through a grant from ARO. The authors made use of shared facilities supported by the NSF MRSEC Program under DMR-0820054.

## REFERENCES

---

<sup>1</sup> For a recent review see D. Talapin, J.S. Lee, M. Kovalenko and E. Shevchenko, *Chem. Rev.* **2010**, *110*, 389.

<sup>2</sup> M. De, P.S. Ghosh, V.M. Rotello, *Adv. Mat.* **2008**, *20*, 4225.

<sup>3</sup> J. Tang and E. H. Sargent, *Adv Mat.* **2011**, *23*, 12.

<sup>4</sup> E. H. Sargent, *Adv. Mat.* **2008**, *20*, 3958.

<sup>5</sup> D.H. Cui, J. Xu, S.Y. J, Xu G. Paradee B.A. Lewis, M.D, Gerhold, *IEEE Trans, Nanotechnology*, **2006**, *5*, 362

<sup>6</sup> G. Konstantatos, I. Howard , A. Fischer, S. Hoogland, J. Clifford, E. Klem, L. Levina, and E. H. Sargent, *Nature* **2006**, *442*, 180.

<sup>7</sup> M. Boberl, M.V. Kovalenko, S. Gamerith, E.J.W. List, W. Heiss, *Adv. Mat.* **2007**, *19*, 3574.

<sup>8</sup> S. Keuleyan, E. Lhuillier, P. Guyot-Sionnest, *J. Am. Chem. Soc.* **2011**, *133*, 16422.

<sup>9</sup> E. Lhuillier, S., Keuleyan, P. Guyot-Sionnest, *Nanotechnology* **2012**, *23*, 175705.

- 
- <sup>10</sup> E. Lhuillier, S. Keuleyan, P. Rekemeyer and P. Guyot-Sionnest, *J. Appl. Phys* **2011**, *110*, 032110.
- <sup>11</sup> D. A. R. Barkhouse, A. G. Pattantyus-Abraham, L. Levina, E. H. Sargent, *ACS Nano* **2008**, *2*, 2356.
- <sup>12</sup> M. Law, J.M. Luther, Q. Song, M.C. Beard, A.J. Nozik, *ACS Nano* **2008**, *2*, 271.
- <sup>13</sup> D. Yu, C.J. Wang, P. Guyot-Sionnest, *Science* **2003**, *300*, 1277.
- <sup>14</sup> Y. Liu, M. Gibbs, C.L. Perkins, M.H. Zarghami, Jr. J. Bustamante, M. Law, *Nano Letters* **2011**, *11*, 5349.
- <sup>15</sup> M. V. Kovalenko, M. Scheele, D.V. Talapin. *Science* **2009**, *324*, 1417.
- <sup>16</sup> A. Nag, M. V. Kovalenko, J.S. Lee, W. Liu, B. Spokoyny, and D. V. Talapin. *J. Am. Chem. Soc.* **2011**, *133*, 10612.
- <sup>17</sup> J. H. Choi, A.T. Fafarman, S.J. Oh, D.K. Ko, D.K. Kim, B.T. Diroll, S. Muramoto, J.G. Gillen, C.B. Murray, C.R. Kagan, *Nano Letter* **2012**, *12*, 2631.
- <sup>18</sup> J. Tang, K. W. Kemp, S. Hoogland, K. S. Jeong, H. Liu, L. Levina, M. Furukawa, X. Wang, R. Debnath, D. Cha, K. W. Chou, A. Fischer, A. Amassian, J. B. Asbury, E. H. Sargent, *Nat. Mater.* **2011**, *10*, 765.
- <sup>19</sup> M.V. Kovalenko, M. I. Bodnarchuk, J. Zaumseil, J.S. Lee, D.V. Talapin, *J. Am. Chem. Soc.* **2010**, *132*, 10085.
- <sup>20</sup> M.V. Kovalenko, M. I. Bodnarchuk, D.V. Talapin *J. Am. Chem. Soc.* **2010**, *132*, 15124.
- <sup>21</sup> M.V. Kovalenko, R.D. Schaller, D. Jarzab, M.A. Loi, D.V. Talapin, *J. Am. Chem. Soc.* **2012**, *134*, 2457.
- <sup>22</sup> S. Keuleyan, E. Lhuillier, V. Brajuskovic, P. Guyot-Sionnest, *Nat. Photon.* **2011**, *5*, 489.
- <sup>23</sup> R. Ihly, J. Tolentino, Y. Liu, M. Gibbs, M. Law, *ACS Nano* **2011**, *5*, 8175.
- <sup>24</sup> C. Tsay, E. Mujagić, C. K. Madsen, C.F. Gmachl and Craig B. Arnold, *Optics Express* **2010**, *18*, 15523.
- <sup>25</sup> H. Kim, K. Cho, D.-W. Kim, H.-R. Lee and S. Kim, *Appl. Phys. Lett.* **2006**, *89*, 173107.
- <sup>26</sup> J. Yun, K. Cho and S. Kim, *Nanotechnology* **2010**, *21*, 235204.
- <sup>27</sup> D. Kim, J. Jang, H. Kim, K. Cho and S. Kim, *Thin Solid Films* **2008**, *516*, 7715.
- <sup>28</sup> H. Liu, S. Keuleyan, P. Guyot-Sionnest *J. Phys. Chem. C* **2012**, *116*, 1344.
- <sup>29</sup> J.D Jensen, R.B. Schoolar, *J. Vac. Sci. Techol* **1976**, *13*, 920.

## **Mid-Infrared HgTe/As<sub>2</sub>S<sub>3</sub> FETs and photodetectors**

### **Supplementary information for:**

## **Mid-Infrared HgTe/As<sub>2</sub>S<sub>3</sub> FETs and photodetectors**

Emmanuel Lhuillier, Sean Keulyan, Pavlo Zolotavin and Philippe Guyot-Sionnest  
James Franck Institute, 929 E. 57<sup>th</sup> Street, The University of Chicago, Chicago, Illinois  
60637, USA

### **Content**

1. Chemical products .....	2
2. Characterization of the HgTe CQD .....	2
3. Setup used for noise measurement. ....	3
4. Effect of AsCl <sub>3</sub> .....	4
5. Effect of As <sub>2</sub> S <sub>3</sub> in air .....	5
6. Effect of oxidation on a sample prepared air free with As <sub>2</sub> S <sub>3</sub> . ....	6
7. Responsivity and detectivity map at 2 μm .....	7

## 1. Chemical products

HgCl<sub>2</sub>, octadecylamine, tellurium powder, Trioctylphosphine, dodecanethiol, tetrachloroethylene, octane, propylamine, ethanedithiol, and ammonium sulfide (Sigma Aldrich), As<sub>2</sub>S<sub>3</sub> (Alfa Aesar), methanol, toluene, hexane (Fisher), ethanol 200 proof (Decon Labs). All reagents are used as purchased.

## 2. Characterization of the HgTe CQD

Figure S 1(a) shows a transmission electron microscopy image (TEM). The structure of the nanoparticle is zinc blende (see X ray diagram on Figure S 1 (b) and their photocurrent spectra show a rather sharp absorption edge, see Figure S 1 (c).

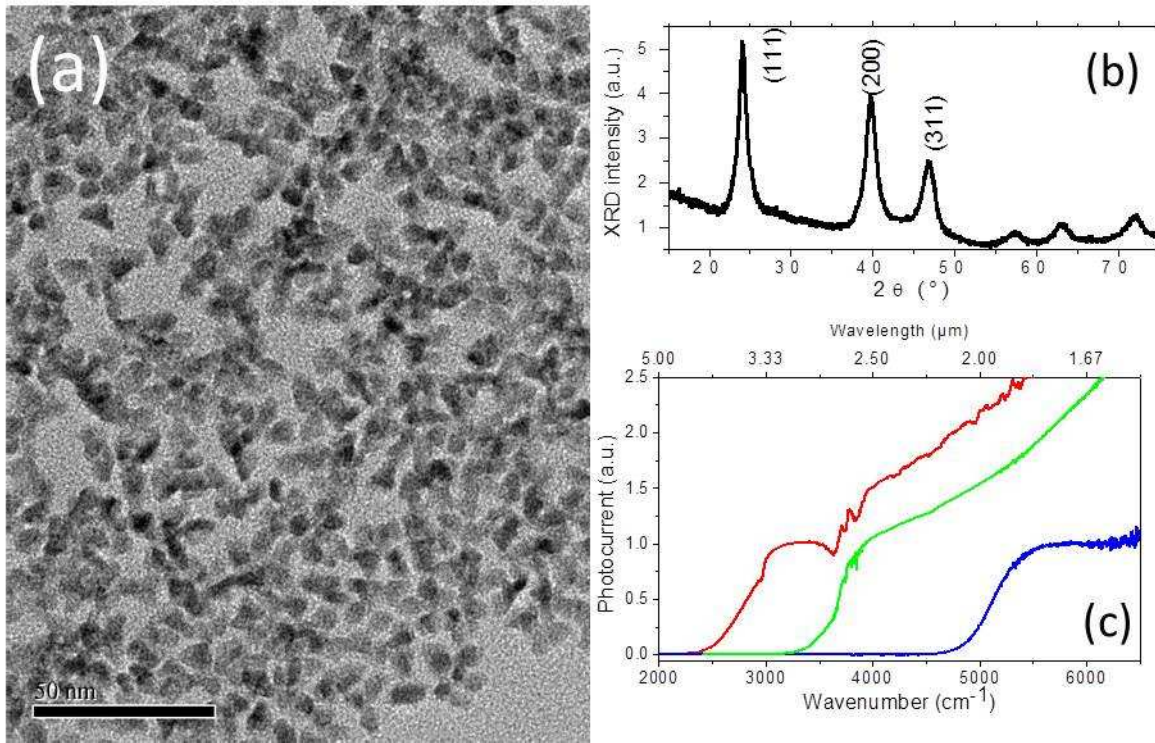


Figure S 1 (a) Transmission electron microscopy picture of HgTe CQD. (b) X ray diffraction diagram of HgTe CQD film. (c) Photocurrent spectra of HgTe CQD films in this study.

### 3. Setup used for noise measurement.

The setup (see Figure S 2) is composed of two magnification stages. After biasing the sample, the current is magnified using a femto DLCPA 200 current amplifier. For quiet systems, the output of this first stage is filtered using a 0.1 Hz high pass filter and the output is amplified by a factor 10. The overall gain of this setup can be adjusted between  $10^3$  and  $10^{10}$ .

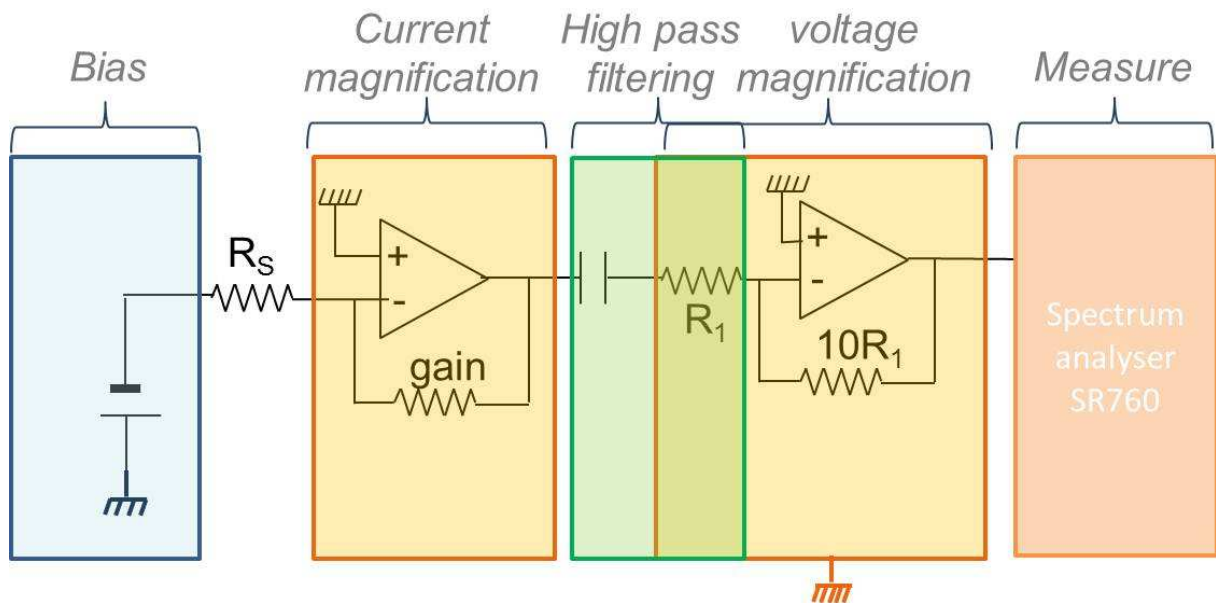


Figure S 2 : setup used for the noise measurements

#### 4. Effect of $\text{AsCl}_3$

We screened different ions for their effect on the HgTe CQD film conductance, and we observe that overall most of them have to effect, except for  $\text{As}^{3+}$  which leads to a huge reduction of the film resistance, see Figure S 3 (a). Nevertheless the I-T curve of a film of HgTe CQD processed with  $\text{As}^{3+}$  still exhibits a non monotonic behavior with a bump around 200K, see Figure S 3 (b). on the other hand the responsivity of the film processed with this method is high (up to  $140\text{mA}\cdot\text{W}^{-1}$ ), which is 100 times higher than the one reported with EDT and as high as the one reported for aggregated material, see Figure S 3 (c). The obtained detectivity can be up to a few  $10^9$ jones.

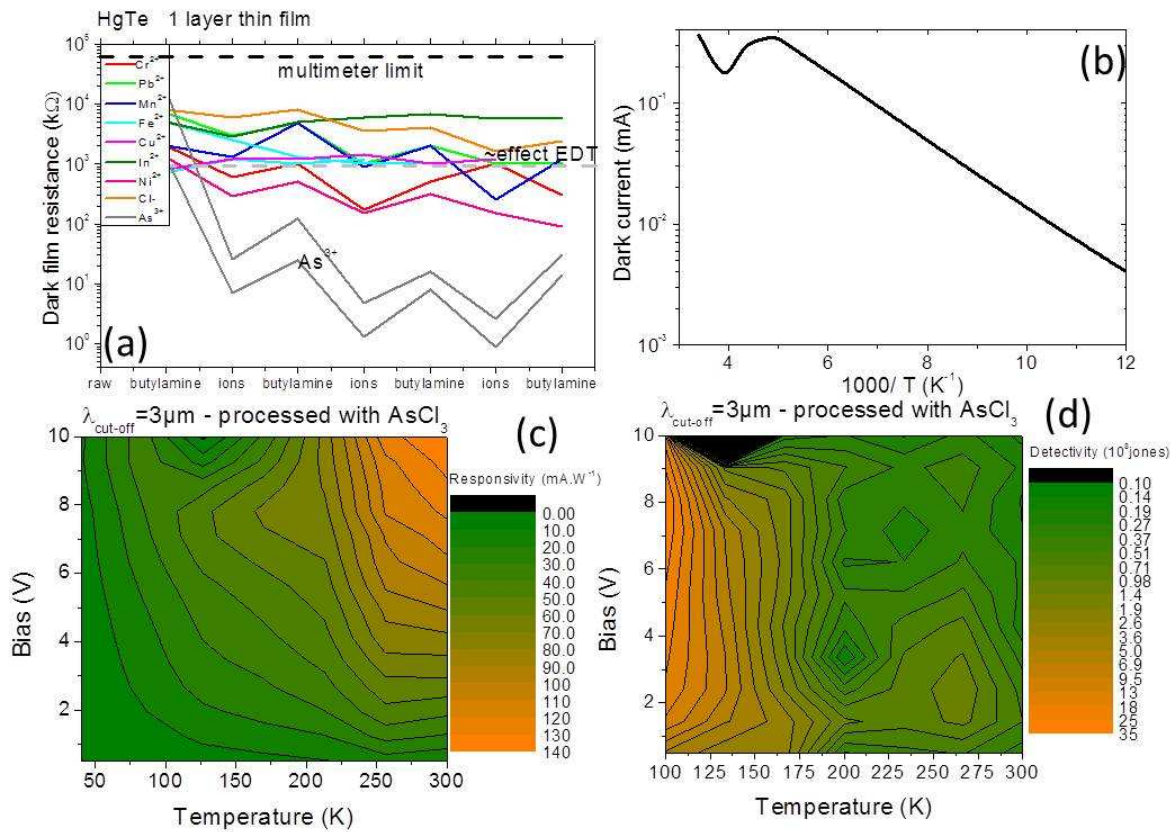


Figure S 3 (a) resistance of a film of HgTe CQD as a function of the process, different ions are tested. (b) Current as a function of the inverse of the temperature of a film of HgTe CQD processed in air with  $\text{AsCl}_3$ . (c) and (d) are the responsivity and detectivity map (as a function of bias and temperature) of a a film of HgTe CQD processed in air with  $\text{AsCl}_3$ .

## 5. Effect of As<sub>2</sub>S<sub>3</sub> in air

Encapsulating the HgTe CQD in As<sub>2</sub>S<sub>3</sub> matrix even in air leads to improved stability with monotonic I(T) curve and improved conductance. This can be explained by a better interparticle coupling. The spectrum is redshifted as the film is dipped for longer times into As<sub>2</sub>S<sub>3</sub>, see Figure S 4 (a). Samples processed in air show extremely slow response time compared to the EDT ligand exchange, see Figure S 4 (c) and (d). The HgTe films can be capped with a layer of pure As<sub>2</sub>S<sub>3</sub>, see Figure S 4 (b), which role is to prevent oxidation of the nanoparticle film.

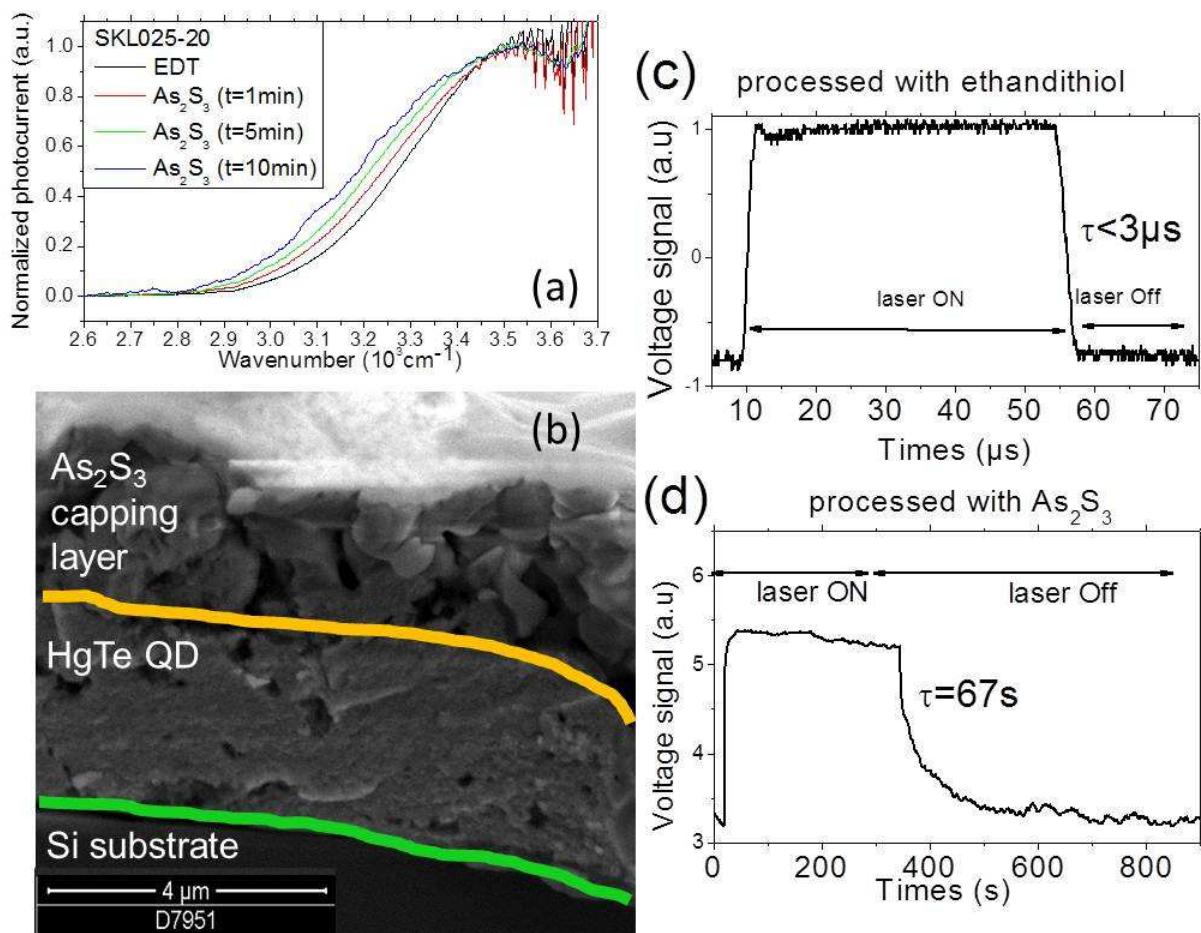


Figure S 4 (a) Photocurrent spectra of a film of HgTe CQD at room temperature treated with ethandithiol and with As<sub>2</sub>S<sub>3</sub> with different duration. (b) scanning electron microscopy picture of a film of HgTe CQD treated with As<sub>2</sub>S<sub>3</sub> with its capping layer of pure As<sub>2</sub>S<sub>3</sub>. (c) Photoreponse of a film of HgTe CQD processed in air with ethandithiol during and after its illumination with a 800nm laser. (d) Photoresponse of a film of HgTe CQD processed in air with As<sub>2</sub>S<sub>3</sub> during to a 800nm laser.

## 6. Effect of oxidation on a sample prepared air free with $\text{As}_2\text{S}_3$ .

A film of HgTe CQD prepared air free with  $\text{As}_2\text{S}_3$  and then exposed to air for several hours still exhibits the same ambipolar behavior, see Figure S 5. This pledges for a better passivation of the HgTe CQD once encapsulated in the inorganic matrix. Nevertheless the on-off ratio is already reduced. No time dependent study of the oxidation has been conducted so far.

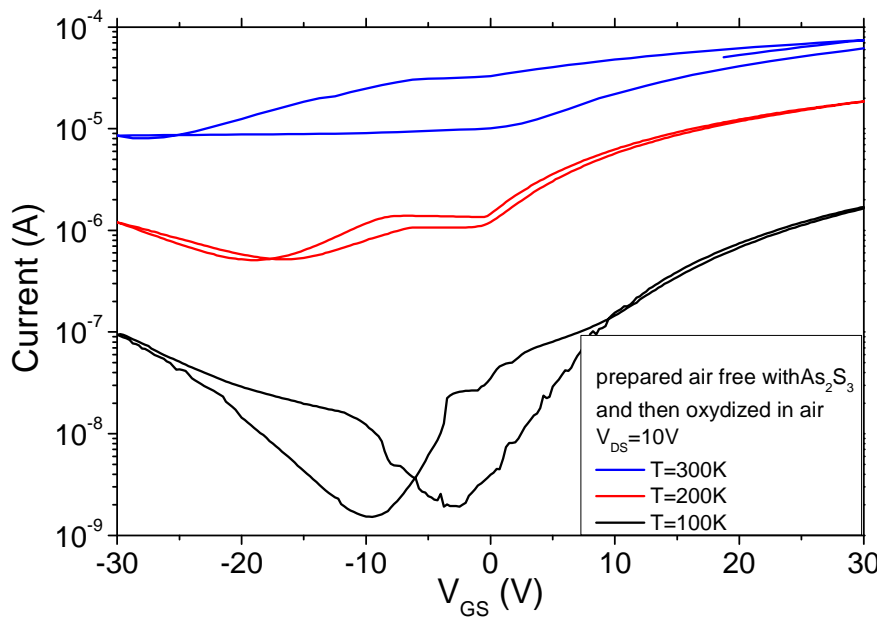


Figure S 5: drain source current as a function of the gate source bias, for a 10V drain source bias at different temperature. The film has been processed in the glove box with  $\text{As}_2\text{S}_3$  and then oxidized by removing the film from its cell and then being heated under heat gun.

## 7. Responsivity and detectivity map at 2 $\mu\text{m}$

We also investigate the effect of the matrix on different batch of HgTe CQD with cut-off wavelength at 2 $\mu\text{m}$ . The associated responsivity and detectivity map are shown on Figure S 6.

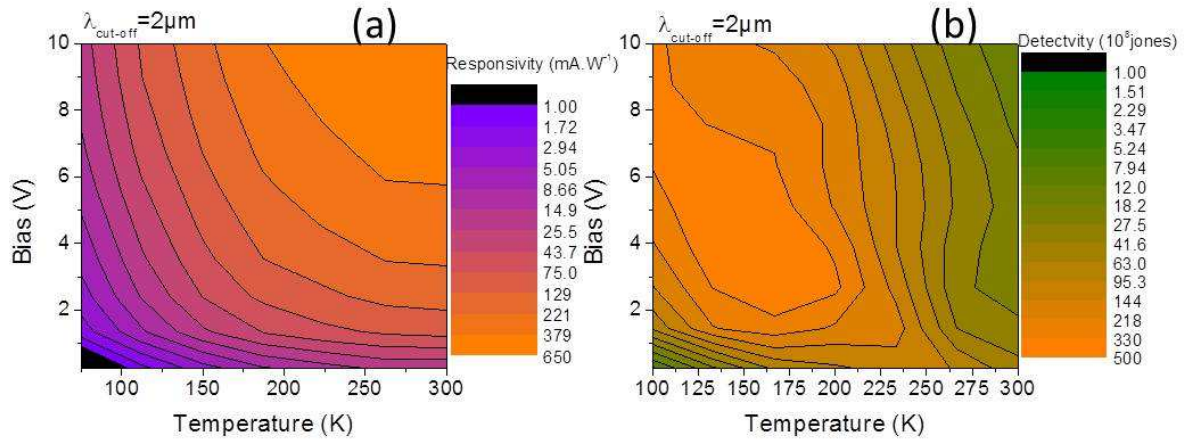


Figure S 6 (a) and (b) are the responsivity and detectivity map as a function of bias and temperature of a film of HgTe CQD treated with  $\text{As}_2\text{S}_3$  and a cut-off wavelength at 2 $\mu\text{m}$ .